

Probabilistic Robustness Analysis for DNNs based on PAC Learning

Renjue Li^{1,2}, Pengfei Yang^{1,2}, Cheng-Chao Huang^{3,4}, Bai Xue^{1,2}, and Lijun Zhang^{1,2,3}

¹ SKLCS, Institute of Software, Chinese Academy of Sciences, Beijing, China

² University of Chinese Academy of Sciences, Beijing, China

³ Institute of Intelligent Software, Guangzhou, China

⁴ CAS Software Testing (Guangzhou) Co., Ltd., Guangzhou, China

Abstract. This paper proposes a black box based approach for analysing deep neural networks (DNNs). We view a DNN as a function f from inputs to outputs, and consider the local robustness property for a given input. Based on scenario optimization technique in robust control design, we learn the score difference function $f_i - f_\ell$ with respect to the target label ℓ and attacking label i . We use a linear template over the input pixels, and learn the corresponding coefficients of the score difference function, based on a reduction to a linear programming (LP) problems. To make it scalable, we propose optimizations including components based learning and focused learning. The learned function offers a probably approximately correct (PAC) guarantee for the robustness property. Since the score difference function is an approximation of the local behaviour of the DNN, it can be used to generate potential adversarial examples, and the original network can be used to check whether they are spurious or not. Finally, we focus on the input pixels with large absolute coefficients, and use them to explain the attacking scenario. We have implemented our approach in a prototypical tool DeepPAC. Our experimental results show that our framework can handle very large neural networks like ResNet152 with 6.5M neurons, and often generates adversarial examples which are very close to the decision boundary.

1 Introduction

Deep neural networks (DNNs) are now widely applied in many applications such as image classification [23], game playing [44], and recently scientific discovery on predictions of protein structure [41]. They are very powerful in performing tasks which are particularly challenging for traditional logic-based software. However, DNNs have been shown to lack robustness [48], i.e., a small or even imperceptible perturbed input can change the classification label. This raises concerns on employing DNNs in safety-critical applications like self-driving cars [51], medical systems [42], and malware detections [26]. It is thus important that robustness of DNNs should be evaluated before they are deployed in safety-critical domains.

We view a DNN as a function f from inputs to outputs, and consider the local robustness property for a given input $\mathbf{x} = (x_1, \dots, x_m)^\top$ consisting of m pixels. It requests that an input sample should have stable output if we add a small perturbation

to it. Stated differently, this holds if $f_i - f_\ell < 0$ for all output label i different from the target label ℓ . Also, if we weaken the condition to allow a small error rate ϵ when we evaluate a robustness property, we obtain a probabilistic robustness (or quantitative robustness) property. Probabilistic robustness matches the idea of label change rate of mutation testing [53, 52] for DNNs, so it can evaluate local robustness very well. When we define a robustness property, there are several different definitions of the perturbations, which lead to different robustness regions. In this paper, we focus on the most commonly used L_∞ robustness, but the method proposed can be extended to other robustness properties.

Testing is an effective approach for analyzing robustness properties. One can simply sample a set of points in the neighborhood of \mathbf{x} , and check whether they all have the same target label ℓ . Testing conducts sampling up to a well-defined convergence criteria, depending on factors such as robustness radius, and computing resources. If a counterexample (adversarial example) is found, surely the property does not hold. But otherwise, the result remains unknown.

In the formal verification community, abstraction based techniques have been successfully applied to non-trivial networks to check $f_i - f_\ell < 0$. The idea is to encode computations of neurons as constraints, and check the robustness property with SMT based solvers, abstract interpretation, or counterexample guided abstraction refinement. If the verification result is affirmative, one can conclude that the network is locally robust. Due to over-approximations in the abstraction based approach, the result may be inconclusive otherwise. The verification tools include Marabou [21], ERAN [46, 47], PRODeep [25], DeepSRGR [61], etc. The state-of-the-art tools can verify DNNs with thousands of neurons. However, the size of DNNs used in real life is far larger, for example, a ResNet [16] has millions of hidden neurons. Recently, abstraction of DNNs have been proposed in [13, 1] to deal with large networks, in which the abstraction models have a strict soundness guarantee. However, these abstraction based methods are still limited on very large DNNs.

In this paper we propose a black box based approach for analyzing deep neural networks (DNN). The idea is inspired by the scenario optimization technique in robust control design, which has been recently applied in probably approximately correct (PAC) learning for hybrid systems [60]. Intuitively, with a pre-specified confidence and error rate, it can infer a function approximating the underlying complex systems. In our setting of robustness, we assume the input image x is classified as target label ℓ , and the attacking label i is often the output label having the second highest score. We learn the *difference function* $\Delta_i = f_i - f_\ell$ with respect to the target label ℓ and attacking label i . We use linear template over the input pixels, i.e., assuming $\tilde{\Delta}_i(\mathbf{x}) = \sum_j c_j x_j$ with x_j the value of a pixel of the input image \mathbf{x} . Further, we sample a set of points near \mathbf{x} and construct constraints of the form $|\Delta_i(\mathbf{x}') - \tilde{\Delta}_i(\mathbf{x}')| \leq \lambda$ for each of the sampled point \mathbf{x}' . In this way, we arrive at a linear programming (LP) problem, and can synthesize the coefficients c_j in the difference function $\tilde{\Delta}_i$.

The above approach is a black box approach in the sense that it depends only on the input m and output n of the DNN, but not their hidden layers. The number of constraints and variables are both in the order of mn . In addition to guaranteeing the error rate ϵ and confidence η , the resulting LP problem has often millions of constraints. To

make it scalable, we propose two optimizations, namely the *component based learning* and *focused learning*. In component based learning, each output is treated separately, and in focused learning, a *two-phase* learning strategy is applied to be able to handle larger input. In the first phase, a small LP is constructed to identify a set of important input features. Then, only the coefficients of those important features will be updated in the second phase. The learned function offers a PAC (probably approximately correct) guarantee for the robustness property. Up to now, works on sampling based probabilistic robustness verification include [54, 55, 3]. The essential difference between our method and these works is that we learn an abstraction model with the error bounded under a PAC guarantee, while previous methods only look at the samples, and the learned abstraction model is able to provide additional insights to the analysis of robustness, especially counterexample generation and model explanation.

Since the learned difference function is a PAC-approximation of the local behaviour of the DNN, it can be used to generate potential adversarial counterexamples. Exploiting the linearity of the learned difference function, we can easily compute the maximum, which is considered as our potential counterexample. The potential counterexample is based on the difference function, which offers a more targeted strategy for generating counterexamples. By identifying similarities of output labels, we select an attacking label i . For instance, we may attack number 8 with 3. We may also choose the second highest score as the attacking label. For the attacking label i , we compute the PAC approximation of $\Delta_i \approx f_i - f_\ell$. We can compute a point x^* achieving the maximum value, allowing us also to synthesize the corresponding input. For such choice, the original network is then used to check whether it is spurious or not, namely whether $f_i - f_\ell > 0$ holds.

Our synthesized PAC approximation provides an effective way to synthesize counterexamples. Moreover, it can also intuitively illustrate the important pixels, thus *explaining* why the attack is successful. To explain the attacking scenario, we visualize the pixels with large absolute coefficients. In this way, we can identify the main features that are useful to original label, and attacking label, respectively.

We have implemented our algorithm in a prototypical tool DeepPAC. Our experimental results are quite promising. For MNIST dataset, comparing to existing tools, DeepPAC can verify larger robustness radii with very high confidence and low error rate. DeepPAC can handle ResNet networks for CIFAR-10 dataset with more than 6.5M neurons, which can hardly be processed by verification tools.

We observe that, DeepPAC can generate adversarial examples very close to the decision boundary, i.e., $f_i > f_\ell$ and $f_i - f_\ell$ is very small. Visualizing the coefficients and counterexamples show that they can capture the essential *differences* of the original and attacking images. Similarly, weighting the input image with their corresponding coefficients highlights the essential features of the image, providing a visual explanation of the attacking scenario.

Organisations of the paper. We provide preliminaries in Sect. 2. An illustrating example is presented in Sect. 3 to show the main idea of function learning. In Sect. 4, we formally introduce our learning algorithm for the abstraction and how to verify a probabilistic robustness property with the abstraction we learn. Counterexample generation is discussed in Sect. 5. The experimental results of abstraction precision, verification per-

formance, and adversarial example generation are presented in Sect. 6. Furthermore, we adopt our method to model explanation and show the explanation of the attacking behaviors on MNIST and CIFAR-10 images. We discuss related works and conclude our work in Sect. 8 and Sect. 9, respectively.

2 Preliminaries

In this section, we recollect some basic concepts on deep neural networks, local robustness verification, and scenario optimization. We denote x_i as the i th entry of a given vector $\mathbf{x} \in \mathbb{R}^m$.

2.1 Deep Neural Network and Local Robustness

Our work concentrates on deep neural networks (DNNs), which can be characterized as a function $\mathbf{f} : \mathbb{R}^m \rightarrow \mathbb{R}^n$. For classification tasks, a DNN usually chooses the output dimension with the largest score, i.e., $C_f(\mathbf{x}) := \arg \max_{1 \leq i \leq n} f_i(\mathbf{x})$, as its output label. A DNN is comprised of layers. The first layer is the input layer, followed by some hidden layers and an output layer in the end. A hidden layer applies an affine transformation or a non-linear activation function on the output of last layer. The function f is the composition of the transformations between layers.

For $\mathbf{x} \in \mathbb{R}^m$, its L_∞ norm is defined as $\|\mathbf{x}\|_\infty := \max_{1 \leq i \leq m} |x_i|$. We use the notation $B(\mathbf{x}, r) := \{\mathbf{x}' \in \mathbb{R}^m \mid \|\mathbf{x} - \mathbf{x}'\|_\infty \leq r\}$ to represent the closed L_∞ ball with center $\mathbf{x} \in \mathbb{R}^m$ and radius $r > 0$. A (local) robustness property of a DNN is defined as follows:

Definition 1 (DNN robustness). *Given a DNN $\mathbf{f} : \mathbb{R}^m \rightarrow \mathbb{R}^n$, an input $\mathbf{x} \in \mathbb{R}^m$, and $r > 0$, we say that \mathbf{f} is (locally) robust at \mathbf{x} with respect to r if for all $\mathbf{y} \in B(\mathbf{x}, r)$, we have $C_f(\mathbf{y}) = C_f(\mathbf{x})$.*

Intuitively, local robustness ensures the consistency of the behaviour of a given input under certain perturbations. In practice, we may not need a strict condition of robustness to ensure that there is no adversarial example around an input \mathbf{x} . A notion of mutation testing is proposed in [53, 52], in which a statistical way is followed to estimate the label change rate of an input, and an input is normal if it has a low *label change rate* on its neighbourhood. This motivates us to give a formal definition of the property showing a low label change rate. Below we recall the definition of *probabilistic robustness* [30].

Definition 2 (DNN probabilistic robustness). *Given a DNN: $\mathbf{f} : \mathbb{R}^m \rightarrow \mathbb{R}^n$, an L_∞ ball $B(\mathbf{x}, r)$, an error rate $\epsilon \in [0, 1)$, and a probability measure \mathbb{P} on $B(\mathbf{x}, r)$, the DNN \mathbf{f} is probabilistic robust at \mathbf{x} with respect to r with the error rate ϵ , if*

$$\mathbb{P}(\{\mathbf{y} \in B(\mathbf{x}, r) \mid C_f(\mathbf{y}) = C_f(\mathbf{x})\}) \geq 1 - \epsilon. \quad (1)$$

By introducing probability, we relax the limitation of local robustness by allowing an error rate ϵ . In this work, we focus on probabilistic local robustness of a given error rate ϵ .

2.2 Scenario Optimization

We provide a brief introduction to scenario optimization. Scenario optimization has been successfully used in robust control design, which attempts to obtain a solution of a class of optimization problems in a statistical sense by only considering a randomly sampled finite subset of infinitely many convex constraints. The optimization problem can be defined as follows:

$$\begin{aligned} & \min_{\gamma \in \Gamma \subseteq \mathbb{R}^m} \mathbf{c}^\top \gamma \\ & \text{s.t. } f_\omega(\gamma) \leq 0, \forall \omega \in \Omega, \end{aligned} \quad (2)$$

where f_ω is a convex and continuous function over the m -dimensional optimization variable γ for every $\omega \in \Omega$. We also assume that both Ω and Γ are convex and closed.

Generally, it is challenging, or even impossible, to solve (2). Calafiore et al. [5] proposed the following scenario approach to provide a solution with a PAC guarantee.

Definition 3. Let \mathbb{P} be a probability measure on Ω . The scenario approach to handle the optimization problem 2 is to solve the following problem. We extract K independent and identically distributed (i.i.d.) samples $(\omega_i)_{i=1}^K$ from Ω according to the probability measure \mathbb{P} :

$$\begin{aligned} & \min_{\gamma \in \Gamma \subseteq \mathbb{R}^m} \mathbf{c}^\top \gamma \\ & \text{s.t. } \bigwedge_{i=1}^K f_{\omega_i}(\gamma) \leq 0. \end{aligned} \quad (3)$$

The scenario approach relaxes the infinitely many constraints in (2) by only considering a finite subset. Previous works (e.g., [6]) have proved a mathematical rigorous relation between the scenario solution and the original constraints in (2).

Theorem 1 ([6]). If (3) is feasible and has a unique optimal solution γ_K^* , and

$$\epsilon \geq \frac{2}{K} \left(\ln \frac{1}{\eta} + m \right), \quad (4)$$

where ϵ and η are the user-defined error rate and the confidence level, respectively, then with confidence at least $1 - \eta$, the optimal γ_K^* satisfies all the constraints in Ω but only at most a fraction of probability measure ϵ , i.e., $\mathbb{P}(f_\omega(\gamma_K^*) > 0) \leq \epsilon$.

The conclusion above still holds if the uniqueness of the optimal γ_K^* is removed, since a unique optimal solution can always be obtained by using the Tie-break rule [5] if more than one optimal solution exists. Hereafter, we set \mathbb{P} to be $U(\Omega)$, the uniform distribution on Ω . The probabilistic guarantee mentioned above is similar to our definition of probabilistic robustness (see Def. 2). We will describe how it can be used verify probabilistic robustness in the following sections.

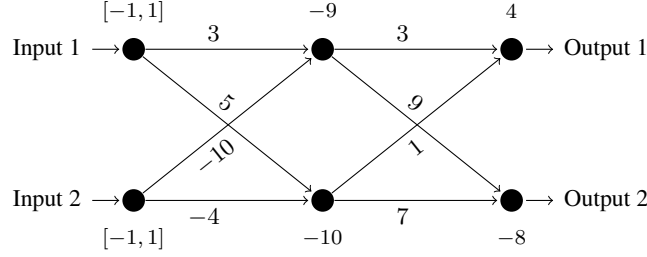


Fig. 1: An FNN with two input neurons, two hidden neurons and two output neurons.

3 An Illustrating Example

The scenario optimization technique has been exploited in the context of *black box* verification for hybrid systems in [60]. We illustrate the main idea, using the feedforward neural network (FNN) as in Fig. 1, where every affine transformation is followed by a ReLU activation function in the hidden layer. It is easy to see that the neural network characterizes a function $\mathbf{f} : \mathbb{R}^2 \rightarrow \mathbb{R}^2$. For an input $\mathbf{x} = (x_1, x_2)^\top \in [-1, 1]^2$, we have $\mathbf{f}(\mathbf{x}) = (f_1(\mathbf{x}), f_2(\mathbf{x}))^\top$.

Assume that at input $\hat{\mathbf{x}} = (0, 0)$, the out label is $C_f(\hat{\mathbf{x}}) = 1$. The network is robust if $f_2(\mathbf{x}) < f_1(\mathbf{x})$ for $\mathbf{x} \in B(\hat{\mathbf{x}}, 1)$, or equivalently, $f_2(\mathbf{x}) - f_1(\mathbf{x}) < 0$. Thus, our goal is to apply the scenario approach to learn the score difference $\Delta(\mathbf{x}) = f_2(\mathbf{x}) - f_1(\mathbf{x})$.

In this example, we take the approximate function of the form $\tilde{\Delta}(\mathbf{x}) = c_0 + c_1x_1 + c_2x_2$ with constant parameters $c_0, c_1, c_2 \in [-100, 100]$ to be synthesized. For simplicity, we denote $\mathbf{c} = (c_1, c_2, c_3)^\top$.

We attempt to approximate $\Delta(\mathbf{x})$ by minimizing the absolute difference between it and the approximate function $\tilde{\Delta}(\mathbf{x})$. This process can be characterized as an optimization problem:

$$\begin{aligned} & \min_{\mathbf{c}, \lambda} \lambda \\ \text{s.t. } & |\tilde{\Delta}(\mathbf{x}) - \Delta(\mathbf{x})| \leq \lambda, \quad \forall \mathbf{x} \in [-1, 1]^2, \\ & \mathbf{c} \in [-100, 100]^3, \\ & \lambda \in [-100, 100]. \end{aligned} \quad (5)$$

To apply the scenario approach, we first need to extract K independent and identically distributed samples $(\mathbf{x}_j)_{j=1}^K$, and then reduce the optimization problem (5) to the following linear programming problem over decision variables \mathbf{c} and λ :

$$\begin{aligned} & \min_{\mathbf{c}, \lambda} \lambda \\ \text{s.t. } & -\lambda \leq \tilde{\Delta}(\mathbf{x}_j) - \Delta(\mathbf{x}_j) \leq \lambda, \quad 1 \leq j \leq K, \\ & \mathbf{c} \in [-100, 100]^3, \\ & \lambda \in [-100, 100]. \end{aligned} \quad (6)$$

According to Theorem 1, it requires at least $\frac{2}{\epsilon}(\ln \frac{1}{\eta} + 4)$ samples to guarantee the confidence at least $1 - \eta$ and the error rate within ϵ , i.e. $\mathbb{P}(|\tilde{\Delta}(\mathbf{x}) - \Delta(\mathbf{x})| \leq \lambda) \geq 1 - \epsilon$. For illustration, below we give two possible initiations of the parameters:

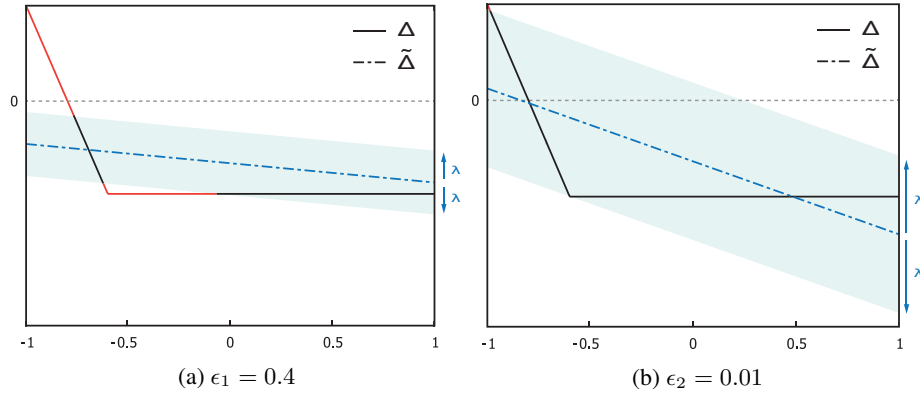


Fig. 2: By fixing $x_1 = 1$, the functions Δ and $\tilde{\Delta}$ are depicted in (a) and (b), respectively. It is marked red where Δ is not bounded by $\tilde{\Delta} \pm \lambda$.

- Taking the error rate $\epsilon = 0.4$ and the confidence $\eta = 0.001$, we need (at least) $K = 55$ samples in $[-1, 1]^2$. By solving the linear programming problem (6), we obtain $c_0 = -11.7720$, $c_1 = 3.6815$, $c_2 = -2.4568$, and $\lambda = 4.074$.
- Taking the error rate $\epsilon = 0.01$ and the confidence $\eta = 0.001$, we need (at least) $K = 2182$ samples in $[-1, 1]^2$. By solving the linear program (3) again, we obtain $c_0 = -10.4051$, $c_1 = 2.800$, $c_2 = -9.095$, and $\lambda = 9.821$.

For illustration, we restrict $x_1 = 1$, and depict the functions Δ and $\tilde{\Delta}$ in Fig. 2. Our goal is to verify that the first output is always larger than the second, i.e., $\Delta(\mathbf{x}) = f_2(\mathbf{x}) - f_1(\mathbf{x}) < 0$. We can analyze it with the learned PAC approximation $\tilde{\Delta}$, which is explained below:

- First we set $\epsilon = 0.4$. As can be seen from Fig. 2(a), $\tilde{\Delta}(\mathbf{x}) + \lambda \leq 0$ at $\mathbf{x} = (1, -1)^\top$. Furthermore, combining the signs of the coefficients of $\tilde{\Delta}$, we obtain that $\tilde{\Delta}(\mathbf{x})$ attains the maximum value at $\mathbf{x} = (1, -1)^\top$ in $[-1, 1]^2$. Therefore, the network is probabilistic robust with respect to 1 with the error rate $\epsilon = 0.4$, i.e., $\mathbb{P}(\Delta(\mathbf{x}) \leq 0) \geq 1 - \epsilon$, with confidence at least $1 - \eta$.
As one can see, the network is actually not robust. However, due to the high error rate, the network is verified to be PAC robust. Interestingly, in this situation the learned function can still guide us to find a real counterexample by substituting the maximum point into the original function.
- Now set $\epsilon = 0.01$. It may not be probabilistic robust, as $\tilde{\Delta}(\mathbf{x}) + \lambda \leq 0$ does not hold. There exists a counterexample (at the point $x_1 = 1$ and $x_2 = -1$).

4 Scenario Optimization based Abstraction

In this section we elucidate our method for analyzing probabilistic robustness of DNNs via learning score difference functions based on scenario optimization. The concept of score difference functions is formally introduced in Sect. 4.1, and two optimization

methods involving component based learning and focused learning are presented in Sect. 4.2 and Sect. 4.3, respectively.

4.1 Learning the Score Difference

Consider a DNN expressed by the function $\mathbf{f} : \mathbb{R}^m \rightarrow \mathbb{R}^n$ with $\mathbf{f} = (f_1, \dots, f_n)^\top$, where f_i denotes the function corresponding to the i th output. Denote by $\ell = C_f(\mathbf{x})$ the classified label of \mathbf{x} .

We aim at learning the *score difference function* $\mathbf{\Delta} = (\Delta_1(\mathbf{x}), \dots, \Delta_n(\mathbf{x}))^\top$ which is defined by

$$\mathbf{\Delta}(\mathbf{x}) = (f_1(\mathbf{x}) - f_\ell(\mathbf{x}), \dots, f_n(\mathbf{x}) - f_\ell(\mathbf{x}))^\top. \quad (7)$$

Here we ignore the entry $f_\ell(\mathbf{x}) - f_\ell(\mathbf{x})$ in (7) and regard the score difference function $\mathbf{\Delta}$ as a function from \mathbb{R}^m to \mathbb{R}^{n-1} . Let $\tilde{\mathbf{\Delta}}(\mathbf{x}) : \mathbb{R}^m \rightarrow \mathbb{R}^{n-1}$ be the function we use to approximate $\mathbf{\Delta}$. In this paper, we assume that each $\tilde{\Delta}_i(\mathbf{x})$ is an affine function with bounded coefficients. A reason for choosing an affine template is that the behaviors of a DNN in a small L_∞ ball $B(\mathbf{x}, r)$ is very close to some affine function. Specifically, for the i th dimension, we set

$$\tilde{\Delta}_i(\mathbf{x}) = \mathbf{c}_i^\top \mathbf{x} = c_{i,0} + c_{i,1}x_1 + \dots + c_{i,m}x_m.$$

With extracting K independent and identically distributed samples $\hat{X} \subset X$, the learning problem aforementioned can be reduce into the following optimization with constraints.

$$\begin{aligned} & \min_{\lambda \geq 0} \lambda \\ \text{s.t. } & -\lambda \leq \mathbf{c}_i^\top \mathbf{x} - \Delta_i(\mathbf{x}) \leq \lambda, \forall \mathbf{x} \in \hat{X}, i \neq \ell, \\ & L \leq \mathbf{c}_{i_k} \leq U, \quad i \neq \ell, k = 0, \dots, m. \end{aligned} \quad (8)$$

In this situation, the problem is restricted to be a linear programming. We assume λ^* being the optimal solutions, and $\tilde{\Delta}_i^*$ being the function $\tilde{\Delta}_i$ when coefficients \mathbf{c}_i are instantiated according to the optimal solution λ^* .

Specifically, we aim to compute a function $\tilde{\mathbf{\Delta}}$ approximating $\mathbf{\Delta}$ with a PAC guarantee:

Definition 4 (PAC Approximation). Let $\mathbf{\Delta} : \mathbb{R}^m \rightarrow \mathbb{R}^n$, and $\epsilon, \eta \in (0, 1]$ be the error rate and confidence, respectively. A function $\tilde{\mathbf{\Delta}} : \mathbb{R}^m \rightarrow \mathbb{R}^n$ is a PAC approximation of $\mathbf{\Delta}$, if

$$\mathbb{P}(\|\tilde{\mathbf{\Delta}}(\mathbf{x}) - \mathbf{\Delta}(\mathbf{x})\|_\infty \leq \lambda) \geq 1 - \epsilon, \quad (9)$$

with confidence at least $1 - \eta$ for a certain radius λ , denoted by $\tilde{\mathbf{\Delta}}(\mathbf{x}) \approx_{\eta, \epsilon, \lambda} \mathbf{\Delta}(\mathbf{x})$.

By Theorem 1, the confidence and the error rate can be ensured by sufficiently large number of the samples. Namely, to make (9) hold with $1 - \eta$ confidence, we can choose any K satisfying

$$K \geq \frac{2}{\epsilon} \left(\ln \frac{1}{\eta} + (m+1)(n-1) + 1 \right) \quad (10)$$

for $(m+1)(n-1) + 1$ variables in (8).

Once we obtain $\tilde{\Delta}(\mathbf{x})$ satisfying (9), we can have a PAC guarantee of the probabilistic robustness. Let X be the input region. We assume $\tilde{\Delta}(\mathbf{x}) \approx_{\eta, \epsilon, \lambda} \Delta(\mathbf{x})$. If $\tilde{\Delta}(\mathbf{x}) + \lambda \leq 0$ for $\mathbf{x} \in X$, then the original network grants probabilistic robustness at \mathbf{x} , i.e., $\mathbb{P}(C_f(\mathbf{x}) = \ell) \geq 1 - \epsilon$ with confidence $1 - \eta$. Formally, note that $\mathbb{P}(C_f(\mathbf{x}) = \ell) = \mathbb{P}(\Delta(\mathbf{x}) \leq 0)$, and we further have

$$\mathbb{P}(\Delta(\mathbf{x}) \leq 0) \geq \mathbb{P}(\Delta(\mathbf{x}) \leq \tilde{\Delta}(\mathbf{x}) + \lambda) \geq \mathbb{P}(\|\tilde{\Delta}(\mathbf{x}) - \Delta(\mathbf{x})\|_\infty \leq \lambda) \geq 1 - \epsilon.$$

It is worth mentioning that, the above framework also works for L_p -norm based robustness with $1 \leq p < \infty$, where we can adopt the gradient descent algorithm to obtain the maximum of $\tilde{\Delta}(\mathbf{x})$ and see whether it is larger than 0.

For fixed η and ϵ , K is in $O(mn)$, so the LP problem (8) contains $O(mn)$ variables and $O(mn^2)$ constraints. However, it is not realistic to apply the LP-based approach directly for high-dimensional inputs and outputs. For example, in the MNIST dataset we have $m = 784$ and $n = 10$. Even for $\eta = 0.001, \epsilon = 0.4$, we need to solve an LP problem with 7065 variables and more than 630000 constraints, which is too consuming in time and space (memory out with 10GB memory). To further make it scale with high-dimensional inputs and outputs, we propose the following optimizations to reduce the complexity of the LP problem.

4.2 Component based Learning

First, we reduce the above LP problems to a few smaller problems. The idea is to learn the functions $\Delta_1, \dots, \Delta_n$ separately, and then combine the solutions together. As before, we use $\tilde{\Delta}_i$ to approximate each $\Delta_i(\mathbf{x}) = |f_i(\mathbf{x}) - f_\ell(\mathbf{x})|$, with the same template. Obviously, instead of solving one big LP problem, we have now $n - 1$ (excluding the one with the target label ℓ) LP problems each with $O(m)$ linear constrains.

Remark 1. Note that $\tilde{\Delta}(\mathbf{x}) \approx_{\eta, \epsilon, \max_i \lambda_i} \Delta(\mathbf{x})$ cannot be deduced from $\tilde{\Delta}_i(\mathbf{x}) \approx_{\eta, \epsilon, \lambda_i} \Delta_i(\mathbf{x})$ for $i \neq \ell$. The confidence of

$$\mathbb{P}\left(\bigwedge_{i \neq \ell} |\tilde{\Delta}_i(\mathbf{x}) - \Delta_i(\mathbf{x})| \leq \lambda_i\right) \geq 1 - \epsilon$$

will decrease at most to $1 - (n - 1)\eta$. This is the reason why the final λ need to be computed from the independent sampling if we want to keep the confidence $1 - \eta$.

A simple solution is to find a new λ . We find it by constructing and solving the following optimization problem:

$$\begin{aligned} & \min_{\lambda} \lambda \\ & \text{s.t. } |\tilde{\Delta}_i(\hat{x}_k) - \Delta_i(\hat{x}_k)| \leq \lambda, \\ & \quad k = 1, \dots, K, i \neq \ell. \end{aligned}$$

where \hat{x}_k are i.i.d $U(X)$ samples and $K \geq \frac{2}{\epsilon}(\ln \frac{1}{\eta} + 1)$. Applying Thm. 1 again, we have $\tilde{\Delta}(\mathbf{x}) \approx_{\eta, \epsilon, \lambda} \Delta(\mathbf{x})$ as desired.

We have already reduced the optimization problem to $n - 1$ smaller LP problems. Let us reconsider our example in Sect. 4.1: Setting parameters $\eta = 0.001, \epsilon = 0.1$, we can solve a smaller linear programming problem in 89.4 seconds with less than 8GB memory; however, for a smaller error rate such as $\epsilon = 0.02$, it takes more than 2 hours and then raises a solver error. Thus we have to reduce the size of the optimization problem further.

4.3 Focused Learning

In previous sections, we have discussed how to approximate each component separately, and reduce the number of constraints in the LP problem from $O(mn^2)$ to $O(m)$. In this subsection, our goal is to reduce the complexity further by dividing the learning procedure into two phases with different fineness. In the first phase, we use a small set of samples to extract coefficients with big absolute values. These coefficients are focused in the second phase, in which we use more samples to refine them. In this way, we reduce the number of variables overall. We call it *focused learning*, which namely refers to focusing the model learning procedure on important features. It is embedded in the component learning procedure.

Considering the i th component, the main idea of focused learning is depicted as follows:

1. *First learning phase:* We sample $K^{(1)}$ i.i.d. samples from the input region $B(\mathbf{x}, r)$. We first learn Δ_i on the $K^{(1)}$ samples. Thus, our LP problems have $O(K^{(1)})$ constraints with $O(m)$ variables. For large datasets like CIFAR-10 and ImageNet, the resulting LP problem is still too large. We use efficient learning algorithms such as linear regression to boost the first learning phase on these large datasets.
2. *Key feature extraction:* After solving the LP problem (or the linear regression for large datasets), we synthesize $\tilde{\Delta}_i^{(1)}$ as the approximate function. Let $KeyF_i(\kappa) \subseteq \{1, x_1, \dots, x_m\}$ denote the set of extracted key features for the i th component corresponding to the largest κ coefficients in $\tilde{\Delta}_i^{(1)}$.
3. *Focused learning phase:* We sample $K^{(2)}$ i.i.d. samples from $B(\mathbf{x}, r)$. For these samples, we generate constraints only for our key features in $KeyF_i(\kappa)$ by fixing the other coefficients using those in $\tilde{\Delta}_i^{(1)}$, and thus the number of the undetermined coefficients is bounded by κ . By solving an LP problem comprised of these constraints, we finally determine the coefficients of the features in $KeyF_i(\kappa)$.

In our experiment, we first determine the sample size $K^{(1)}$ and $K^{(2)}$, and then choose the largest κ satisfying

$$\kappa \leq \frac{K^{(2)}\epsilon}{2} - \ln \frac{1}{\eta} - 1,$$

which can be easily inferred from Theorem 1.

5 Counterexample Generation

We have discussed how to synthesize an affine function $\tilde{\Delta}$ over the key features to approximate the score difference function Δ . In this section, we exploit our abstraction $\tilde{\Delta}$ for counterexample generation.

Definition 5. Let $\ell = C_f(\mathbf{x})$. We say $\mathbf{x}^* \in B(\mathbf{x}, r)$ is a counterexample in $B(\mathbf{x}, r)$ with respect to a label $i \neq \ell$, if $\Delta_i(\mathbf{x}^*) > 0$, or equivalently, $f_i(\mathbf{x}^*) > f_\ell(\mathbf{x}^*)$.

When the optimization problem is solved, for the optimal solution $\tilde{\Delta}(\mathbf{x})$, $\tilde{\Delta}(\mathbf{x}) \pm \lambda$ is the approximation of its upper/lower bound with PAC guarantee. Actually, if \mathbf{x}^* satisfies $\tilde{\Delta}_i(\mathbf{x}^*) + \lambda > 0$, it is a potential counterexample attacking the classification label ℓ using i . We describe below the idea for finding counterexamples:

1. For an input \mathbf{x} , we first compute its label ℓ . We synthesize $\tilde{\Delta}_i^*$ using focused learning in Sect. 4.
2. Since $\tilde{\Delta}_i^*(\mathbf{x}) = c_0 + \sum_j c_j x_j$ is an affine function, we can infer the optimal \mathbf{x}^* directly as

$$x_j^* = \begin{cases} x_j + r, & c_j > 0, \\ x_j - r, & c_j \leq 0. \end{cases}$$

Here for the case $c_j = 0$, the choice of x_j^* is arbitrary, and we choose $x_j - r$ as an instance.

3. If $f_i(\mathbf{x}^*) > f_\ell(\mathbf{x}^*)$, we return \mathbf{x}^* it as a real counterexample. Otherwise, it is a *spurious counterexample*, in which case we change the attacking label i and go to Step 1.

We note that the above procedure may be non-conclusive, in which case the result is unknown. Moreover, the maximal value of $\tilde{\Delta}_i^*$ may not correspond to the maximal value of Δ_i , which is illustrated in the following example.

Example 1. We use two FNNs to demonstrate different situations. Suppose the property we want to verify is that the first output is always larger than the second. In both examples, we set the error rate $\epsilon = 0.01$ and the confidence level $\eta = 0.001$. We show the results in Fig. 3.

- Fig. 3(a) corresponds to the network in Sect. 3. According to $\tilde{\Delta}(\mathbf{x})$ we learn, the potential counterexample generated is $\mathbf{x}^* = (1, -1)^\top$. It is a true counterexample.
- For the network in Fig. 4, we use the same linear template $\tilde{\Delta}(\mathbf{x}) = c_0 + c_1 x_1 + c_2 x_2$ to approximate the corresponding $\Delta(\mathbf{x}) = f_2(\mathbf{x}) - f_1(\mathbf{x})$ with $\eta = 0.001$ and $\epsilon = 0.01$. By solving the linear programming problem (6), we can obtain $c_0 = -43.9568, c_1 = 26.1851, c_2 = -4.7748, \lambda = 21.9271$, and the result is shown in Fig. 3(b). At this time, the potential counterexample we generated is still $\mathbf{x}^* = (1, -1)^\top$, as it corresponds to the maximum of our approximation. It can be easily checked that it is a spurious counterexample. However, the original network is unsafe, as can be easily observed from Fig. 3(b).

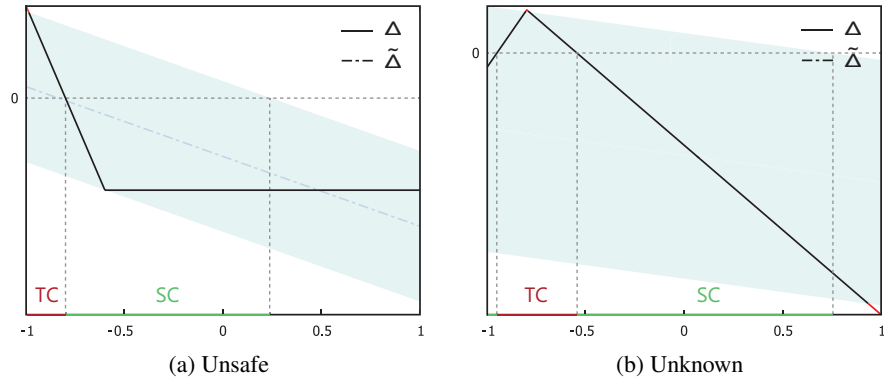


Fig. 3: Counterexample generation results. We fix $x_1 = 1$. TC and SC refer to *true counterexample* and *spurious counterexample*, respectively. In (a), the maximum point of the learned function is a real counterexample, whereas in (b), it is spurious.

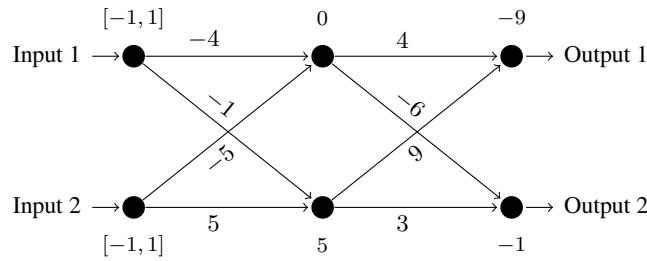


Fig. 4: The network has the same structure but different parameters as the one in Fig. 1. However, we find a spurious counterexample.

6 Experiments

We implement our approach as a prototype called DeepPAC. The implementation is based on Python 3.7.8. We use CVXPY [10] as the modeling language for linear programming and GUROBI [15] as the LP solver. All experiments are conducted on a Windows 10 PC with Intel i7 8700, GTX 1660Ti, and 16G RAM.

Datasets. The MNIST [24] database contains greyscale pictures of handwritten numbers with 60 000 images for training and 10 000 for testing. The image size of the MNIST database is 28×28 . The CIFAR-10 [22] dataset contains color images in ten classes. Every class has 5 000 images for training and 1 000 images for testing. The image size of the CIFAR-10 dataset is 32×32 . Both datasets are used in image classification. Before training, we normalized both the MNIST dataset and the CIFAR-10 dataset and performed random cropping and horizontal flipping during CIFAR-10 training.

Index	Network	ERAN (DeepPoly)	$\epsilon = 0.05$			$\epsilon = 0.01$			$\epsilon = 0.001$		
			✓	?	×	✓	?	×	✓	?	×
0	FNN 1	2	4	5	6	4	5	6	4	5	6
	FNN 2	3	5	6	7	5	6	7	5	6	7
	FNN 3	4	9	–	10	9	–	10	9	–	10
	FNN 4	4	11	–	12	11	–	12	11	–	12
	FNN 5	6	22	–	23	22	–	23	22	–	23
	FNN 6	3	10	–	11	10	–	11	10	–	11
128	FNN 1	4	7	[8,9]	10	7	[8,9]	10	7	[8,9]	10
	FNN 2	7	23	[24,31]	32	23	[24,31]	32	23	[24,30]	31
	FNN 3	6	27	28	29	26	[27,28]	29	26	[27,28]	29
	FNN 4	4	21	[22,24]	25	21	[22,24]	25	21	[22,24]	25
	FNN 5	5	50	–	51	50	–	51	51	–	52
	FNN 6	3	25	–	26	25	–	26	25	–	26
256	FNN 1	4	9	10	11	9	10	11	9	10	11
	FNN 2	5	12	–	13	12	–	13	12	–	13
	FNN 3	5	13	–	14	13	–	14	13	–	14
	FNN 4	3	16	–	17	16	–	17	16	–	17
	FNN 5	3	22	–	23	21	22	23	21	22	23
	FNN 6	3	15	–	16	15	–	16	15	–	16

Table 1: Verification results of MNIST. The column for ERAN provides the maximal robustness radius that ERAN can verify. In the headline, “✓” is the maximal PAC radius we can check, “×” offers the smallest radius such that DeepPAC can generate a counterexample, “?” indicates the unknown range of the radius, and “–” means that the item is empty.

Networks. On MNIST, we trained six feedforward networks named from FNN1 to FNN6 with the structures of varying numbers of hidden layers and hidden neurons in each layer: 3×50 , 3×100 , 6×200 , 9×200 , and 6×500 . We used the stochastic gradient descent optimizer with a learning rate of 0.001. For the CIFAR-10 dataset, we trained a large convolutional neural network [45] (VGG16) and four residual neural networks [16] (ResNet18, ResNet50, ResNet101, ResNet152). The number of parameters are 14.7M, 11.2M, 23.5M, 42.5M and 58.2M respectively. The stochastic gradient descent optimizer is still used for training, using 0.1, 0.01, and 0.001 as the learning rate successively, and each learning rate is trained for 200 epochs.

6.1 Maximal Robust Radius

For the verification task, we first pick the 0-th, 128-th, and 256th images in the MNIST training set, and verify them with $\eta = 99.9\%$ confidence and error rates of $\epsilon = 0.05$, 0.01, and 0.001, respectively. We invoke our *focused learning algorithm*, and use binary search to find a relatively large robust radius r so that it is PAC robust, and a relatively small unsafe radius. It should be noted that because of the existence of probability, the binary search may not be stable, and the result is obtained by fixing the random seed.

Network	Image 0			Image 128			Image 256		
	$r = 1$	$r = 2$	$r = 5$	$r = 1$	$r = 2$	$r = 5$	$r = 1$	$r = 2$	$r = 5$
VGG16	✓	×	×	✓	×	×	✓	✓	×
ResNet18	✓	×	×	✓	×	×	✓	✓	×
ResNet50	✓	×	×	×	×	×	✓	?	×
ResNet101	✓	?	×	×	×	×	✓	✓	×
ResNet152	×	×	×	×	×	×	✓	?	?

Table 2: CIFAR-10 verification result. With $\eta = 99.9\%$ confidence and error rates of $\epsilon = 0.01$, we verify the CIFAR-10 nets using radii 1, 2 and 5.

Comparison with ERAN. We compare with state-of-the-art tool ERAN [47], and use the DeepPoly abstract domain to verify the networks and record the maximum robust radius that can be verified. The maximum robust radius is given in the practical sense (a grayscale value from 0 to 255). The corresponding results of the three error rates are shown in Table 1.

ERAN is an abstract interpretation based tool, which is a soundness approach. Namely, its error rate can be regarded as zero. Besides, the precision loss of the abstract interpretation method increases with the depth of the neural network. Therefore, it is conceivable that ERAN always has a smaller robustness radius than our method. For instance FNN6 and the 256th image, our PAC verified robustness radius is 5-times larger than the one guaranteed by ERAN.

When using DeepPAC, the robustness radius obtained shows obvious differences on different networks. But for ERAN, it remains more or less the same. It is interesting to note that, the network FNN5 has larger robustness radii on the three images than the other networks. From a quantitative perspective, the radius of probabilistic robustness computed by DeepPAC has relatively better practical meanings.

Effect of Focused Learning. In our experiments, we have always invoked our *focused learning optimization*. When the error rate is 0.05 and 0.01, we use the first batch of $K^{(1)} = 2\,000$ random samples and the second batch of $K^{(2)} = 8\,000$ random samples. When the error rate is 0.001, we use the first batch of $K^{(1)} = 8\,000$ random samples and the second batch of $K^{(2)} = 20\,000$ random samples. Overall, the running times are 90, 140, and 300 seconds for error rate 0.05, 0.01 and 0.001 respectively.

It is interesting to observe that our method obtains similar results under different error rates. When we reduce the error rate from 0.05 to 0.01, most of the results agree, but we observe two cases where the PAC-safe radius decreases: they are FNN3 for the 128th image and FNN5 for the 256th image. As is illustrated by our running example (see Fig. 2), a larger error rate may lead to a PAC claim, even when the original network is not robust.

We observe that our framework is not very sensitive to the error bound. One possible reason is that the affine template could converge well under the training with a relatively small batch of samples. Thus our method can learn a good approximation even at a relatively high error bound. It also supports us to reduce the number of samples accordingly to extract the key features in the first phase.

Scalability of DeepPAC. Compared with previous tools based on SMT solvers and abstract interpretations, our method has better scalability. While these tools are white box approach, ours is a black-box approach. We only care about the relationship between input and output, the internal structure of the network has almost no effect on efficiency. Thus, DeepPAC can verify networks much larger than previous methods. On the CIFAR-10 data set, we trained 5 very large neural networks and verified them with our method. It can be seen from Table 4 that our method is still effective on larger data sets and networks.

The tool ERAN supports GPUPoly [32], DeepPoly running on GPUs. GPUPoly can verify a ResNet18 network in an average time of 1 021 seconds with an Nvidia Tesla V100 GPU support, while DeepPAC can analyze a ResNet18 network in 120 seconds using a PC with Intel i7 8700, GTX 1660Ti and 16G RAM. Our framework scales, as it can handle larger networks such as ResNet152 network within three minutes.

6.2 Counterexample Generation

In this section, we report experiments of counterexamples generation using our tool. If the attack class score of the potential counterexample is higher than the correct class, it can be determined that a true counterexample is generated. Our experiment generates counterexamples under the corresponding radii based on the minimum unsafe radii given in previous section (see the column “ \times ” in Table 1).

Mask Image. A counterexample can be considered as an input which is obtained by adding a mask to the original picture. A mask image for the MNIST dataset is a black-and-white image. Black pixels are negative to attack if the value on these pixels increases, and vice versa for white pixels. On CIFAR-10, a mask image is a color image, and each pixel can be seen as an RGB triple. In the counterexample, if the corresponding channel value increases, the channel in the mask is set to 255, or otherwise 0. For example, when the red and green channels of a pixel increases, and the blue channel decreases, then the triple of the pixel is (255, 255, 0), and the color is thus yellow.

MNIST Counterexamples for the networks FNN1–FNN6. The original picture is the 0th image, representing the number 5 shown in Fig. 5. For FNN1–FNN6, we use radii 6, 7, 10, 12, 23, and 11 (see column for $\epsilon = 0.01$ of Table 1). We use the output corresponding to the number 3 to attack it. Fig. 5 shows the counterexamples and masks of the corresponding radius of different networks on the original picture depicted above. We measure the score difference as a quality of the counterexample: the score difference should tend to zero when it is closer to the decision boundary. We observe that the difference is below 1 for five of them, and it is 2.7 for FNN4.

CIFAR-10 Counterexamples for VGG16 and ResNets. Similarly, we have performed experiments on CIFAR-10 dataset. The original picture is the 128th image depicting a dog. Setting $\epsilon = 0.01$, we use radius 2 for VGG16 and ResNet18, and radius 1 for other networks (see the column for Image 128 of Table. 2). We use the output corresponding to the cat to *attack* it. The corresponding results are given in Fig. 6. It shows that almost all networks have poor robustness, as counterexamples can be generated with relatively

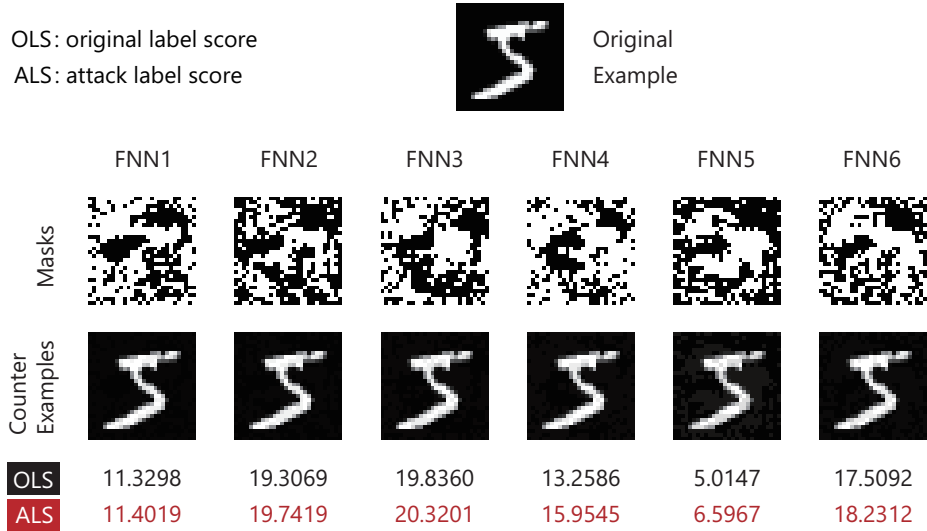


Fig. 5: Counterexamples of neural networks for MNIST. We use the 0th image as the original image. The radii are 6, 7, 10, 12, 23, and 11. The OLS (original label score w.r.t. 5) and ALS (attacking label score w.r.t. 3) are given below.

small radii. Moreover, the difference of the OLS and ALS scores is rather large: it is more than 6 for all counterexamples, and is more than ten times larger for the VGG16.

Mask Image Using Important Pixels. We recall that focused learning optimization allows us to concentrate on those pixels with larger coefficients. In our counterexample generation scheme (see Sect. 5), within the allowed radius, we take the image whose distance is the largest in every pixel. Inspired by focused learning optimization, some pixels may have little effect on the attack. Thus, we now investigate properties of counterexamples when restricting to the set of pixels contributing most.

Assume that we use the output i to attack our image, and we have $\tilde{\Delta}_i(\mathbf{x}) = c_{i0} + \sum_j c_{i,j}x_j$. For pixel x_j , its contribution to the function $\tilde{\Delta}_i(\mathbf{x})$ is *approximately* $c_{i,j}r$. The precise score of the pixel should take account of the fact that pixel value has minimum 0 and maximum 255, so the precise score can be given by $Score(x_j) = \max(c_{i,j} \cdot \min(255 - x_j, r), -c_{i,j} \cdot \min(x_j, r))$. Our strategy is to determine the smallest number of pixels to change based on the contribution of each pixel. The result is shown in Fig. 7. The mask in Fig. 7 has three colors, among which black and white are similar to those in Fig. 5, and the gray pixels mean that the corresponding pixels in the counterexample remain unchanged.

Experimental results are given in Fig. 7. For networks from FNN1 to FNN6, we only need to modify 56.9%, 36.6%, 42.9%, 33.4%, 32.0%, and 46.4%, respectively, of the most important pixels from the original pictures. The successfully generated counterexamples confirms that some pixels that have little effect on the attack. At the same time, the mask image is more recognizable. It can be observed that the counterexample

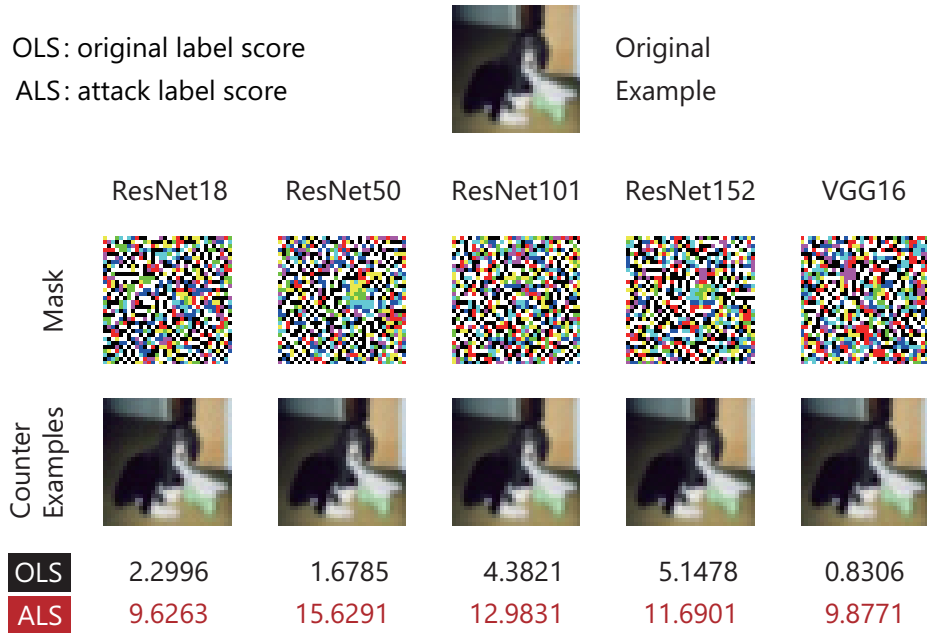


Fig. 6: Counterexamples of neural networks for CIFAR-10. We use the 128th image as the original image. The radii are 1, 1, 1, 2, and 2, respectively. OLS means the original label score w.r.t. the class dog and ALS means the attacking label score w.r.t. the class cat.

darkens the pixel regarding the true value and adds disturbance to the surroundings. We achieve very small score differences for the counterexamples, which are at most 0.02 in these cases. In other words, the counterexample generated in this way is very close to the decision boundary.

7 Explanation of Attacking

In this section, we use our learned functions to give key features for classification and attacking with a given label as a local explanation. With the explanation, we can see which pixels make the most contribution to protecting the classification label from the attack and which tend to make the attack possible.

The model we learn approximates the behaviour of the neural network in a local area surrounding \mathbf{x}^* . We have chosen affine functions as templates, so the absolute value of the synthesized coefficients indicate how much the corresponding pixel values affect the score difference. Recall this is also the essential idea exploited in our focused learning optimization. The positive or negative of the coefficient indicates the direction of the influence of this input dimension on the neural network. What we learned is the score difference of the neural network, i.e. $\Delta_i(\mathbf{x}) = f_i(\mathbf{x}) - f_\ell(\mathbf{x})$, where i corresponds to the output label used to attack the network. Stated differently, we want to generate

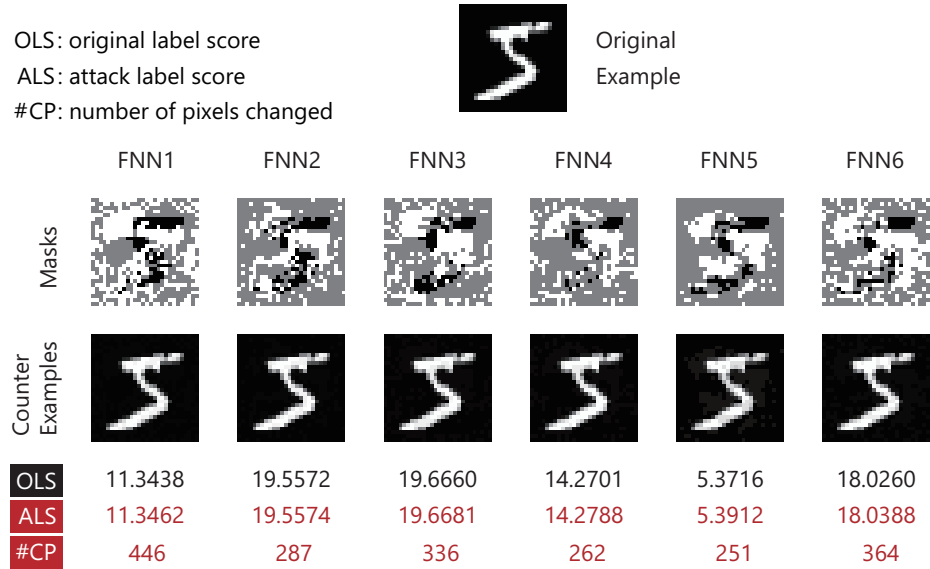


Fig. 7: Counterexamples of neural networks for MNIST with least important pixels changed. The #CP (number of pixels changed) is given below the ALS.

an input so that $f_i(\mathbf{x}) > f_\ell(\mathbf{x})$. We start from our approximate function $\tilde{\Delta}_i(\mathbf{x}) = c_0 + \sum_i c_i x_i$. The absolute value $|c_i|$ of the coefficient c_i determines the influence of the current pixel on the classification result. Note that $f_i(\mathbf{x})$ can be approximated by $f_\ell(\mathbf{x}) + \tilde{\Delta}_i(\mathbf{x}) = f_\ell(\mathbf{x}) + c_0 + \sum_i c_i x_i$. Thus we have

- if $c_i > 0$, increasing it will enlarge the value of $\tilde{\Delta}_i(\mathbf{x})$ corresponding to x_i , which is beneficial to the attacking label, whereas
- if $c_i < 0$, increasing it will reduce the value of $\tilde{\Delta}_i(\mathbf{x})$, which is beneficial to the classification label.

Visualization of the Coefficients for MNIST. Intuitively, the larger the absolute value of the coefficient is, the more important the corresponding pixel is. There is simple way to visualize it by normalizing each coefficient to a value in $[0, 255]$. We visualize the positive and negative coefficients separately as follows:

- Visualizing Negative Coefficients (VNC): The column VNC shows the normalized image in which bright pixels are negative to attack of the target label if the value of these pixels increases. The weighted VNC is obtained by VNC multiplied by the original image pixel wise. Its visualization intuitively shows which pixels are significantly negative to attack.
- Visualizing Positive Coefficients (VPC): Oppositely, the column VPC shows the normalized image in which bright pixels are positive to attack of the target label

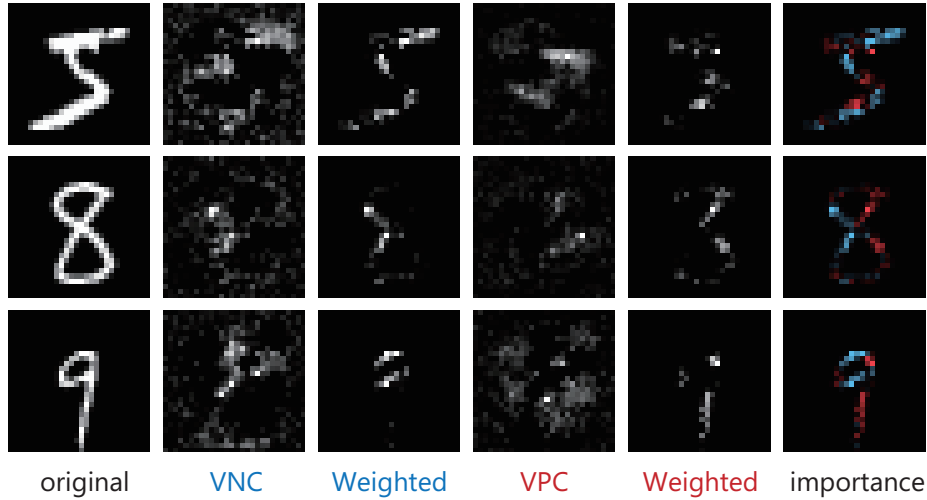


Fig. 8: Explanation of FNN5 for MNIST. The target labels are 5, 8 and 9. The corresponding attack labels are 3, 3 and 1. It visualizes the normalized coefficients (VPC, VNC), and the resulting weighted images.

if the value of these pixels increases. Similarly, the weighted VPC shows which pixels are significantly positive to attack.

In Fig. 8, we illustrate the visualization for three images in MNIST. For instance, the left part of the number “8” are the most bright on weighted VNC, so the pixels in this part are the key features to the classification of “8” against “3”, while on weighted VPC bright pixels lie mostly in the right part, and they are attempting hardest to make the original image classified as “3”. From the aspect of human beings, this explanation is quite fantastic since the right part (weighted VPC) indeed looks like a number “3”, and the left part (weighted VNC) makes the image no longer “3” in our eyes.

Visualization of the Coefficients for CIFAR-10. Unlike MNIST, the CIFAR-10 dataset is in color, and the brightness (the value of the pixels) does not have a close connection to the existence of the object to be recognized. Actually, the coefficients multiplied by pixel values do not provide meaningful image.

The color pixel has three channels and each channel has an independent coefficient, so each pixel has three coefficients, (c_1, c_2, c_3) , for each of the channel respectively. We take the L_2 norm and compute $(c_1^2 + c_2^2 + c_3^2)^{\frac{1}{2}}$ as a measure of the pixel. Using the measure, we mask the image by removing 20%, 40%, 60%, and 80% of the less important pixels. Fig. 9 shows the results on CIFAR-10. We observe that the resulting picture values the part around the head more than others. We anticipate that the horse and airplane have the same *attacking preference*, as no essential differences can be observed. Interestingly, we observe masked image for ResNet152 is more scattered than VGG16.

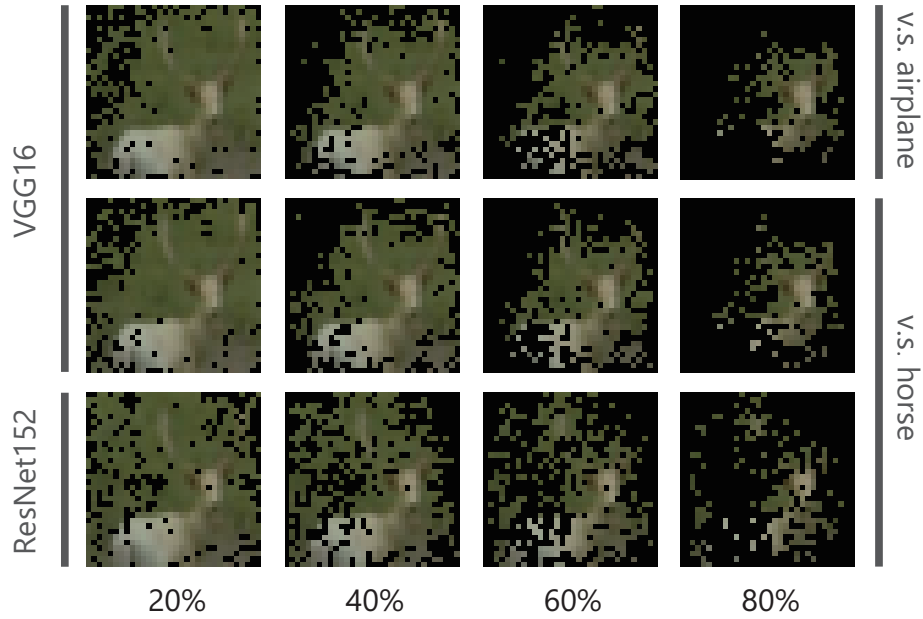


Fig. 9: Explanation of VGG16 and ResNet152 for CIFAR-10. The target label is deer. The attacking labels are airplane and horse, respectively.

8 Related Works

We have already discussed papers mostly related to the present one. Here we add some more new results on verification, model explanation and adversarial attacks for DNNs.

Verification. Alternative approaches based on constraint-solving [20, 12, 28, 33, 4, 27], layer-by-layer exhaustive search [17], global optimization [38, 11, 39], functional approximation [56], reduction to two-player games [57, 58], and star set based abstraction [50, 49] have been proposed as well.

Model explanation. In [2], model explanation was first proposed to describe the local behaviors of a given DNN, and LIME [35] gave an algorithm which learns an affine function based on sampling to describe the local behaviors of DNNs. The difference between our method and LIME is that the error is bounded with a PAC guarantee in our settings, and that we can further explain the attacking behaviors. Subsequent works like [43, 29, 40, 8, 14, 36] provide more algorithms to make model explanation more effective in specific domains.

Adversarial attacks. Adversarial examples and adversarial attacks were first put forward in [48]. The most well-known robustness attack methods include Fast Gradient Sign [31], Jacobian-based saliency map approach [34], C&W attack [7], etc. In recent years a great number of works like [19, 9, 59, 37, 18, 62] have developed adversarial attack with a variety of methods and techniques.

9 Conclusion

We proposed a framework of DNN abstraction for analyzing probabilistic robustness of DNNs in a local region based on scenario optimization. The error between the abstraction model and the original network is bounded with a PAC guarantee. With the abstraction model we learn, we could verify probabilistic robustness properties under given confidence and error rate and generate potential counterexamples for DNN. What's more, the abstraction model is effective on model explanation, especially explaining local attacking behaviors. Experimental results showed that our method scales well on large networks, and has outstanding performance on verification, adversarial example generation and model explanation.

As for future works, it is a natural idea to extend affine functions in our abstraction model to a more complex one. e.g., DNNs or neural networks with random weights so as to further improve the precision of the abstraction. We are also looking for possibility to modify our model explanation framework and adopt it to specific application domains document classification and game playing.

References

1. Ashok, P., Hashemi, V., Kretínský, J., Mohr, S.: Deepabstract: Neural network abstraction for accelerating verification. In: Hung, D.V., Sokolsky, O. (eds.) Automated Technology for Verification and Analysis - 18th International Symposium, ATVA 2020, Hanoi, Vietnam, October 19-23, 2020, Proceedings. Lecture Notes in Computer Science, vol. 12302, pp. 92–107. Springer (2020). https://doi.org/10.1007/978-3-030-59152-6_5, https://doi.org/10.1007/978-3-030-59152-6_5
2. Baehrens, D., Schroeter, T., Harmeling, S., Kawanabe, M., Hansen, K., Müller, K.: How to explain individual classification decisions. *J. Mach. Learn. Res.* **11**, 1803–1831 (2010)
3. Baluta, T., Chua, Z.L., Meel, K.S., Saxena, P.: Scalable quantitative verification for deep neural networks. *CoRR* **abs/2002.06864** (2020), <https://arxiv.org/abs/2002.06864>
4. Bunel, R., Lu, J., Turkaslan, I., Torr, P.H.S., Kohli, P., Kumar, M.P.: Branch and bound for piecewise linear neural network verification. *J. Mach. Learn. Res.* **21**, 42:1–42:39 (2020)
5. Calafiore, G.C., Campi, M.C.: The scenario approach to robust control design. *IEEE Trans. Autom. Control.* **51**(5), 742–753 (2006). <https://doi.org/10.1109/TAC.2006.875041>, <https://doi.org/10.1109/TAC.2006.875041>
6. Campi, M.C., Garatti, S., Prandini, M.: The scenario approach for systems and control design. *Annu. Rev. Control.* **33**(2), 149–157 (2009). <https://doi.org/10.1016/j.arcontrol.2009.07.001>, <https://doi.org/10.1016/j.arcontrol.2009.07.001>
7. Carlini, N., Wagner, D.: Towards evaluating the robustness of neural networks. In: Security and Privacy (SP), 2017 IEEE Symposium on. pp. 39–57. IEEE (2017)
8. Chattopadhyay, A., Sarkar, A., Howlader, P., Balasubramanian, V.N.: Grad-cam++: Generalized gradient-based visual explanations for deep convolutional networks. In: 2018 IEEE Winter Conference on Applications of Computer Vision, WACV 2018, Lake Tahoe, NV, USA, March 12-15, 2018. pp. 839–847. IEEE Computer Society (2018). <https://doi.org/10.1109/WACV.2018.00097>, <https://doi.org/10.1109/WACV.2018.00097>

9. Croce, F., Hein, M.: Reliable evaluation of adversarial robustness with an ensemble of diverse parameter-free attacks. CoRR **abs/2003.01690** (2020), <https://arxiv.org/abs/2003.01690>
10. Diamond, S., Boyd, S.: CVXPY: A Python-embedded modeling language for convex optimization. *Journal of Machine Learning Research* **17**(83), 1–5 (2016)
11. Dutta, S., Jha, S., Sankaranarayanan, S., Tiwari, A.: Output range analysis for deep feedforward neural networks. In: Dutle, A., Muñoz, C.A., Narkawicz, A. (eds.) *NASA Formal Methods - 10th International Symposium, NFM 2018, Newport News, VA, USA, April 17-19, 2018, Proceedings. Lecture Notes in Computer Science*, vol. 10811, pp. 121–138. Springer (2018)
12. Ehlers, R.: Formal verification of piece-wise linear feed-forward neural networks. In: *15th International Symposium on Automated Technology for Verification and Analysis (ATVA2017)*. pp. 269–286 (2017)
13. Elboher, Y.Y., Gottschlich, J., Katz, G.: An abstraction-based framework for neural network verification. In: Lahiri, S.K., Wang, C. (eds.) *Computer Aided Verification - 32nd International Conference, CAV 2020, Los Angeles, CA, USA, July 21-24, 2020, Proceedings, Part I. Lecture Notes in Computer Science*, vol. 12224, pp. 43–65. Springer (2020)
14. Guo, W., Mu, D., Xu, J., Su, P., Wang, G., Xing, X.: LEMNA: explaining deep learning based security applications. In: Lie, D., Mannan, M., Backes, M., Wang, X. (eds.) *Proceedings of the 2018 ACM SIGSAC Conference on Computer and Communications Security, CCS 2018, Toronto, ON, Canada, October 15-19, 2018*. pp. 364–379. ACM (2018)
15. Gurobi Optimization, L.: Gurobi optimizer reference manual (2021), <http://www.gurobi.com>
16. He, K., Zhang, X., Ren, S., Sun, J.: Deep residual learning for image recognition. In: *2016 IEEE Conference on Computer Vision and Pattern Recognition, CVPR 2016, Las Vegas, NV, USA, June 27-30, 2016*. pp. 770–778. IEEE Computer Society (2016). <https://doi.org/10.1109/CVPR.2016.90>, <https://doi.org/10.1109/CVPR.2016.90>
17. Huang, X., Kwiatkowska, M., Wang, S., Wu, M.: Safety verification of deep neural networks. In: *29th International Conference on Computer Aided Verification (CAV2017)*. pp. 3–29 (2017)
18. Huang, Z., Zhang, T.: Black-box adversarial attack with transferable model-based embedding. In: *8th International Conference on Learning Representations, ICLR 2020, Addis Ababa, Ethiopia, April 26-30, 2020*. OpenReview.net (2020), <https://openreview.net/forum?id=SJxhNTNYwB>
19. Kang, X., Song, B., Du, X., Guizani, M.: Adversarial attacks for image segmentation on multiple lightweight models. *IEEE Access* **8**, 31359–31370 (2020). <https://doi.org/10.1109/ACCESS.2020.2973069>, <https://doi.org/10.1109/ACCESS.2020.2973069>
20. Katz, G., Barrett, C.W., Dill, D.L., Julian, K., Kochenderfer, M.J.: Reluplex: An efficient SMT solver for verifying deep neural networks. In: *29th International Conference on Computer Aided Verification (CAV2017)*. pp. 97–117 (2017)
21. Katz, G., Huang, D.A., Ibeling, D., Julian, K., Lazarus, C., Lim, R., Shah, P., Thakoor, S., Wu, H., Zeljic, A., Dill, D.L., Kochenderfer, M.J., Barrett, C.W.: The marabou framework for verification and analysis of deep neural networks. In: Dillig, I., Tasiran, S. (eds.) *Computer Aided Verification - 31st International Conference, CAV 2019, New York City, NY, USA, July 15-18, 2019, Proceedings, Part I. Lecture Notes in Computer Science*, vol. 11561, pp. 443–452. Springer (2019)
22. Krizhevsky, A.: Learning multiple layers of features from tiny images. University of Toronto (05 2012)

23. Krizhevsky, A., Sutskever, I., Hinton, G.E.: Imagenet classification with deep convolutional neural networks. In: *Advances in Neural Information Processing Systems 25: 26th Annual Conference on Neural Information Processing Systems 2012. Proceedings of a meeting held December 3-6, 2012, Lake Tahoe, Nevada, United States.* pp. 1106–1114 (2012)
24. LéCun, Y., Bottou, L., Bengio, Y., Haffner, P.: Gradient-based learning applied to document recognition. *Proceedings of the IEEE* **86**(11), 2278–2324 (1998)
25. Li, R., Li, J., Huang, C., Yang, P., Huang, X., Zhang, L., Xue, B., Hermanns, H.: Prodeep: a platform for robustness verification of deep neural networks. In: Devanbu, P., Cohen, M.B., Zimmermann, T. (eds.) *ESEC/FSE '20: 28th ACM Joint European Software Engineering Conference and Symposium on the Foundations of Software Engineering, Virtual Event, USA, November 8-13, 2020.* pp. 1630–1634. ACM (2020)
26. Li, Y., Xiong, K., Chin, T., Hu, C.: A machine learning framework for domain generation algorithm-based malware detection. *IEEE Access* **7**, 32765–32782 (2019)
27. Lin, W., Yang, Z., Chen, X., Zhao, Q., Li, X., Liu, Z., He, J.: Robustness verification of classification deep neural networks via linear programming. In: *IEEE Conference on Computer Vision and Pattern Recognition, CVPR 2019, Long Beach, CA, USA, June 16-20, 2019.* pp. 11418–11427. Computer Vision Foundation / IEEE (2019)
28. Lomuscio, A., Maganti, L.: An approach to reachability analysis for feed-forward ReLU neural networks. In: *KR2018* (2018)
29. Lundberg, S.M., Lee, S.: A unified approach to interpreting model predictions. In: Guyon, I., von Luxburg, U., Bengio, S., Wallach, H.M., Fergus, R., Vishwanathan, S.V.N., Garnett, R. (eds.) *Advances in Neural Information Processing Systems 30: Annual Conference on Neural Information Processing Systems 2017, December 4-9, 2017, Long Beach, CA, USA.* pp. 4765–4774 (2017)
30. Mangal, R., Nori, A.V., Orso, A.: Robustness of neural networks: A probabilistic and practical approach. *CoRR* **abs/1902.05983** (2019), <http://arxiv.org/abs/1902.05983>
31. Moosavi-Dezfooli, S., Fawzi, A., Frossard, P.: Deepfool: A simple and accurate method to fool deep neural networks. In: *2016 IEEE Conference on Computer Vision and Pattern Recognition, CVPR 2016, Las Vegas, NV, USA, June 27-30, 2016.* pp. 2574–2582. IEEE Computer Society (2016). <https://doi.org/10.1109/CVPR.2016.282>, <https://doi.org/10.1109/CVPR.2016.282>
32. Müller, C., Singh, G., Püschel, M., Vechev, M.T.: Neural network robustness verification on gpus. *CoRR* **abs/2007.10868** (2020), <https://arxiv.org/abs/2007.10868>
33. Narodyska, N., Kasiviswanathan, S.P., Ryzhyk, L., Sagiv, M., Walsh, T.: Verifying properties of binarized deep neural networks. In: McIlraith, S.A., Weinberger, K.Q. (eds.) *Proceedings of the Thirty-Second AAAI Conference on Artificial Intelligence, (AAAI-18), the 30th innovative Applications of Artificial Intelligence (IAAI-18), and the 8th AAAI Symposium on Educational Advances in Artificial Intelligence (EAAI-18), New Orleans, Louisiana, USA, February 2-7, 2018.* pp. 6615–6624. AAAI Press (2018)
34. Papernot, N., McDaniel, P.D., Jha, S., Fredrikson, M., Celik, Z.B., Swami, A.: The limitations of deep learning in adversarial settings. In: *IEEE European Symposium on Security and Privacy, EuroS&P 2016, Saarbrücken, Germany, March 21-24, 2016.* pp. 372–387. IEEE (2016). <https://doi.org/10.1109/EuroSP.2016.36>, <https://doi.org/10.1109/EuroSP.2016.36>
35. Ribeiro, M.T., Singh, S., Guestrin, C.: "why should I trust you?": Explaining the predictions of any classifier. In: Krishnapuram, B., Shah, M., Smola, A.J., Aggarwal, C.C., Shen, D., Rastogi, R. (eds.) *Proceedings of the 22nd ACM SIGKDD International Conference on Knowledge Discovery and Data Mining, San Francisco, CA, USA, August 13-17, 2016.* pp. 1135–1144. ACM (2016)

36. Ribeiro, M.T., Singh, S., Guestrin, C.: Anchors: High-precision model-agnostic explanations. In: McIlraith, S.A., Weinberger, K.Q. (eds.) Proceedings of the Thirty-Second AAAI Conference on Artificial Intelligence, (AAAI-18), the 30th innovative Applications of Artificial Intelligence (IAAI-18), and the 8th AAAI Symposium on Educational Advances in Artificial Intelligence (EAAI-18), New Orleans, Louisiana, USA, February 2-7, 2018. pp. 1527–1535. AAAI Press (2018), <https://www.aaai.org/ocs/index.php/AAAI/AAAI18/paper/view/16982>
37. Ru, B., Cobb, A.D., Blaas, A., Gal, Y.: Bayesopt adversarial attack. In: 8th International Conference on Learning Representations, ICLR 2020, Addis Ababa, Ethiopia, April 26-30, 2020. OpenReview.net (2020), <https://openreview.net/forum?id=Hkem-lrtvH>
38. Ruan, W., Huang, X., Kwiatkowska, M.: Reachability analysis of deep neural networks with provable guarantees. In: IJCAI2018. pp. 2651–2659 (2018)
39. Ruan, W., Wu, M., Sun, Y., Huang, X., Kroening, D., Kwiatkowska, M.: Global robustness evaluation of deep neural networks with provable guarantees for the hamming distance. In: Kraus, S. (ed.) Proceedings of the Twenty-Eighth International Joint Conference on Artificial Intelligence, IJCAI 2019, Macao, China, August 10-16, 2019. pp. 5944–5952. ijcai.org (2019)
40. Selvaraju, R.R., Cogswell, M., Das, A., Vedantam, R., Parikh, D., Batra, D.: Grad-cam: Visual explanations from deep networks via gradient-based localization. In: IEEE International Conference on Computer Vision, ICCV 2017, Venice, Italy, October 22-29, 2017. pp. 618–626. IEEE Computer Society (2017). <https://doi.org/10.1109/ICCV.2017.74>, <https://doi.org/10.1109/ICCV.2017.74>
41. Senior, A.W., Evans, R., Jumper, J., Kirkpatrick, J., Sifre, L., Green, T., Qin, C., Židek, A., Nelson, A.W.R., Bridgland, A., Penedones, H., Petersen, S., Simonyan, K., Crossan, S., Kohli, P., Jones, D.T., Silver, D., Kavukcuoglu, K., Hassabis, D.: Improved protein structure prediction using potentials from deep learning. *Nat.* **577**(7792), 706–710 (2020). <https://doi.org/10.1038/s41586-019-1923-7>, <https://doi.org/10.1038/s41586-019-1923-7>
42. Sheikhtaheri, A., Sadoughi, F., Dehaghi, Z.H.: Developing and using expert systems and neural networks in medicine: A review on benefits and challenges. *J. Medical Syst.* **38**(9), 110 (2014)
43. Shrikumar, A., Greenside, P., Kundaje, A.: Learning important features through propagating activation differences. In: Precup, D., Teh, Y.W. (eds.) Proceedings of the 34th International Conference on Machine Learning, ICML 2017, Sydney, NSW, Australia, 6-11 August 2017. Proceedings of Machine Learning Research, vol. 70, pp. 3145–3153. PMLR (2017)
44. Silver, D., Huang, A., Maddison, C.J., Guez, A., Sifre, L., van den Driessche, G., Schrittwieser, J., Antonoglou, I., Panneershelvam, V., Lanctot, M., Dieleman, S., Grewe, D., Nham, J., Kalchbrenner, N., Sutskever, I., Lillicrap, T.P., Leach, M., Kavukcuoglu, K., Graepel, T., Hassabis, D.: Mastering the game of go with deep neural networks and tree search. *Nature* **529**(7587), 484–489 (2016)
45. Simonyan, K., Zisserman, A.: Very deep convolutional networks for large-scale image recognition. In: Bengio, Y., LeCun, Y. (eds.) 3rd International Conference on Learning Representations, ICLR 2015, San Diego, CA, USA, May 7-9, 2015, Conference Track Proceedings (2015), <http://arxiv.org/abs/1409.1556>
46. Singh, G., Gehr, T., Mirman, M., Püschel, M., Vechev, M.T.: Fast and effective robustness certification. In: Advances in Neural Information Processing Systems 31: Annual Conference on Neural Information Processing Systems 2018, NeurIPS 2018, 3-8 December 2018, Montréal, Canada. pp. 10825–10836 (2018)
47. Singh, G., Gehr, T., Püschel, M., Vechev, M.T.: An abstract domain for certifying neural networks. *PACMPL* **3**(POPL), 41:1–41:30 (2019)

48. Szegedy, C., Zaremba, W., Sutskever, I., Bruna, J., Erhan, D., Goodfellow, I., Fergus, R.: Intriguing properties of neural networks. In: International Conference on Learning Representations (ICLR2014) (2014)
49. Tran, H., Bak, S., Xiang, W., Johnson, T.T.: Verification of deep convolutional neural networks using imagestars. In: Lahiri, S.K., Wang, C. (eds.) Computer Aided Verification - 32nd International Conference, CAV 2020, Los Angeles, CA, USA, July 21-24, 2020, Proceedings, Part I. Lecture Notes in Computer Science, vol. 12224, pp. 18–42. Springer (2020)
50. Tran, H., Lopez, D.M., Musau, P., Yang, X., Nguyen, L.V., Xiang, W., Johnson, T.T.: Star-based reachability analysis of deep neural networks. In: ter Beek, M.H., McIver, A., Oliveira, J.N. (eds.) Formal Methods - The Next 30 Years - Third World Congress, FM 2019, Porto, Portugal, October 7-11, 2019, Proceedings. Lecture Notes in Computer Science, vol. 11800, pp. 670–686. Springer (2019)
51. Urmson, C., Whittaker, W.: Self-driving cars and the urban challenge. *IEEE Intell. Syst.* **23**(2), 66–68 (2008)
52. Wang, J., Dong, G., Sun, J., Wang, X., Zhang, P.: Adversarial sample detection for deep neural network through model mutation testing. In: 2019 IEEE/ACM 41st International Conference on Software Engineering (ICSE). pp. 1245–1256. IEEE (2019)
53. Wang, J., Sun, J., Zhang, P., Wang, X.: Detecting adversarial samples for deep neural networks through mutation testing. *CoRR* **abs/1805.05010** (2018), <http://arxiv.org/abs/1805.05010>
54. Webb, S., Rainforth, T., Teh, Y.W., Kumar, M.P.: A statistical approach to assessing neural network robustness. In: 7th International Conference on Learning Representations, ICLR 2019, New Orleans, LA, USA, May 6-9, 2019. OpenReview.net (2019)
55. Weng, L., Chen, P., Nguyen, L.M., Squillante, M.S., Boopathy, A., Oseledets, I.V., Daniel, L.: PROVEN: verifying robustness of neural networks with a probabilistic approach. In: Chaudhuri, K., Salakhutdinov, R. (eds.) Proceedings of the 36th International Conference on Machine Learning, ICML 2019, 9-15 June 2019, Long Beach, California, USA. Proceedings of Machine Learning Research, vol. 97, pp. 6727–6736. PMLR (2019)
56. Weng, T.W., Zhang, H., Chen, H., Song, Z., Hsieh, C.J., Boning, D., Dhillon, I.S., Daniel, L.: Towards Fast Computation of Certified Robustness for ReLU Networks. In: ICML 2018 (Apr 2018)
57. Wicker, M., Huang, X., Kwiatkowska, M.: Feature-guided black-box safety testing of deep neural networks. In: Beyer, D., Huisman, M. (eds.) Tools and Algorithms for the Construction and Analysis of Systems - 24th International Conference, TACAS 2018, Held as Part of the European Joint Conferences on Theory and Practice of Software, ETAPS 2018, Thessaloniki, Greece, April 14-20, 2018, Proceedings, Part I. Lecture Notes in Computer Science, vol. 10805, pp. 408–426. Springer (2018)
58. Wu, M., Wicker, M., Ruan, W., Huang, X., Kwiatkowska, M.: A game-based approximate verification of deep neural networks with provable guarantees. *Theor. Comput. Sci.* **807**, 298–329 (2020)
59. Xu, J., Du, Q.: Texttricker: Loss-based and gradient-based adversarial attacks on text classification models. *Eng. Appl. Artif. Intell.* **92**, 103641 (2020). <https://doi.org/10.1016/j.engappai.2020.103641>, <https://doi.org/10.1016/j.engappai.2020.103641>
60. Xue, B., Zhang, M., Easwaran, A., Li, Q.: PAC model checking of black-box continuous-time dynamical systems. *IEEE Trans. Comput. Aided Des. Integr. Circuits Syst.* **39**(11), 3944–3955 (2020). <https://doi.org/10.1109/TCAD.2020.3012251>, <https://doi.org/10.1109/TCAD.2020.3012251>
61. Yang, P., Li, R., Li, J., Huang, C., Wang, J., Sun, J., Xue, B., Zhang, L.: Improving neural network verification through spurious region guided refinement. *CoRR* **abs/2010.07722** (2020), <https://arxiv.org/abs/2010.07722>

62. Zhao, C., Fletcher, P.T., Yu, M., Peng, Y., Zhang, G., Shen, C.: The adversarial attack and detection under the fisher information metric. In: The Thirty-Third AAAI Conference on Artificial Intelligence, AAAI 2019, The Thirty-First Innovative Applications of Artificial Intelligence Conference, IAAI 2019, The Ninth AAAI Symposium on Educational Advances in Artificial Intelligence, EAAI 2019, Honolulu, Hawaii, USA, January 27 - February 1, 2019. pp. 5869–5876. AAAI Press (2019). <https://doi.org/10.1609/aaai.v33i01.33015869>, <https://doi.org/10.1609/aaai.v33i01.33015869>